Green Chemistry

PAPER

View Article Online
View Journal | View Issue

Cite this: *Green Chem.*, 2022, **24**, 9697

An eco-friendly, low-cost, and automated strategy for phosphoproteome profiling†

Wenyang Zhang, ‡[a] Cheuk-Kuen Lai,‡[b] Wenjie Huang,[a] Wenyan Li,[a] Shaowen Wu,[a] Qian Kong,[a] Alan C. Hopkinson,[b] Alisdair R. Fernie,[c] K. W. Michael Siu*[b,d] and Shijuan Yan *[a]

Received 22nd June 2022,
Accepted 21st November 2022

DOI: 10.1039/d2gc02345h

rsc.li/greenchem

Reversible protein phosphorylation plays a vital role in many biological processes. In current phosphoproteomics, targeted enrichment before mass spectrometry (MS) analysis is essential. Many kinds of materials have been developed for phosphopeptide enrichment, but these typically involve complex fabrication process and high consumption of chemicals. Furthermore, the enrichment of phosphopeptides is offline and requires multiple manual steps, thereby making it a tedious workflow with high consumption of organic solvents and plastic consumables. To alleviate these problems, we propose a set of eco-friendly strategies for phosphoproteome profiling by developing a reusable phos-trap column *via* a one-pot mild sol–gel process and establishing an automated online analytical platform with low cost and low waste. This platform also demonstrated high phosphosite coverage, sensitivity, selectivity, and a wide linear range when a standard phosphoprotein (α-casein) was used for the initial development assessment. In subsequent analyses of HeLa cells and maize seedlings, a total of 6575 and 3741 phosphorylation sites were characterized, respectively, using three single-shot technical replicates for each sample type with excellent qualitative and quantitative reproducibility. Taken together, this phos-trap column and automated online analytical platform are expected to bring environmental and low-cost technological advancements to phosphoproteomics, especially for large-scale tasks.

1. Introduction

Posttranslational phosphorylation plays key roles in the regulation of protein activity and is involved in many cellular processes, including but not limited to signal transduction and cell division, proliferation, differentiation, transformation and metabolism.[1] As such, global characterization of phosphoproteins and phosphorylation sites would aid in our overall understanding of cellular regulation. Liquid chromatography coupled with tandem mass spectrometry (LC-MS/MS) has become a powerful tool in comprehensive proteome characterization due to its high-sensitivity and high-throughput capabilities.[2] However, it is often impractical to directly characterize phosphopeptides from whole-cell digests by LC-MS/MS due to low phosphopeptide abundance, low ionization efficiency, and signal suppression by non-phosphopeptides. These undesirable features invariably necessitate selective enrichment of phosphopeptides prior to analyses of such peptides.[3]

To date, several enrichment strategies have proven effective, including the employment of immobilized metal ion affinity chromatography (IMAC),[4,5] metal oxide affinity chromatography (MOAC).[6,7] However, the synthesis processes of these materials were complex, usually required several steps of chemical derivatization, and inevitably used a lot of organic solvents.[8,9] In addition, these IMAC materials could not be reused, leading to a serious waste of resources.[10] Offline enrichment of phosphopeptides prior to MS analysis is tedious and labor-intensive, consuming a lot of organic solvents, plastic tubes and pipette tips. Some automatic methods have recently been developed to either simplify or parallelize the enrichment for saving labor. For example, the EasyPhos platform parallelizes protein digestion, desalting and enrichment,[11] whilst AssayMAP Bravo automates the enrichment using a robotic liquid handling platform.[12] However, these methods were still implemented offline and did not help reduce the cost and consumption of reagents and consum-

[a]*Guangdong Key Laboratory for Crop Germplasm Resources Preservation and Utilization, Agro-biological Gene Research Center, Guangdong Academy of Agricultural Sciences, Guangzhou 510640, China. E-mail: shijuan@agrogene.ac.cn*
[b]*Department of Chemistry and Centre for Research in Mass Spectrometry, York University, Toronto, Ontario, M3J 1P3, Canada*
[c]*Max Planck Institute of Molecular Plant Physiology, Am Muhlenberg 1, 14476 Potsdam-Golm, Germany*
[d]*Department of Chemistry and Biochemistry, University of Windsor, Windsor, Ontario, N9B 3P4, Canada. E-mail: kwmsiu@uwindsor.ca*
†Electronic supplementary information (ESI) available. See DOI: https://doi.org/10.1039/d2gc02345h
‡Equal contribution.

ables. With the development of phosphoproteomics towards large-scale tasks, it is urgently necessary to develop a strategy with excellent analytical performance while meeting the requirements of low reagent and consumable consumption.

In this work, we synthesized a novel and reusable phos-trap column for online enrichment of phosphopeptides *via* a "one-pot" process which was easy, eco-friendly, and low-waste. We further integrated it with a commercial nanoLC-MS/MS system without complicated components. Under software control, the platform can automatically and continuously enrich and analyze phosphopeptides from a batch of biological samples without operator intervention. It not only obtains results with high phosphosite coverage and reproducibility, but also excels in characterizing peptides with different phosphorylation states and thereby facilitating the discovery of novel phosphosites. More importantly, the reusable phos-trap columns and online enrichment in a nano-flow device greatly help reduce the consumption of consumables, solvents and save labor in phosphoproteomic studies.

2. Experimental procedures

2.1 Reagents and materials

LC-MS grade acetonitrile (ACN), water, methanol, acetone, formic acid (FA), trifluoroacetic acid (TFA), protease and phosphatase inhibitor mini tablets, bicinchoninic acid (BCA) protein assay, Pierce™ peptide desalting spin columns, C18 pre-column (100 μm I.D. × 20 mm, 5 μm, 164564), C18 analytical column (75 μm I.D. × 150 mm, 3 μm, 164568), 250 μL Syringe Upgrade Kits (6820.0031) were obtained from Thermo Fisher Scientific (MA, USA). $ZrCl_4$, Tris-Cl, EDTA, sucrose, and phenol were obtained from Sinopharm (Shanghai, China). α-Casein, bovine serum albumin (BSA), disodium adenosine 5′-triphosphate ($ATPNa_2$), (3-glycidyloxypropyl)trimethoxysilane (GLYMO), dithiothreitol (DTT), tris(2-carboxyethyl)phosphine (TCEP), iodoacetamide (IAA), urea, NH_4HCO_3, 2,5-dihydroxybenzoic acid (DHB), lactic acid (LA), $NH_4H_2PO_4$ were acquired from Sigma-Aldrich (MO, USA). Potassium silicate solution (40 degrees Baume, 3.3 modulus) was purchased from Shandong Yusuo Chemical Technology Co., LTD. Fused silica capillary tubing (150 μm I.D., 363 μm O.D.) was acquired from Polymicro Technologies. Sequencing-grade trypsin was commercially available from Promega Corporation (WI, USA). SilicaTips Emitter (FS360-20-10-N-20) was obtained from New Objective (MA, USA). HeLa cells (iCell-h088, obtained from iCell Bioscience Inc.) and maize (B73) seedlings were cultured in-house.

The mixer mill (MM400) was obtained from RETSCH (Germany). The sonicator (Bioruptor UCD-300) was obtained from Diagenode (Belgium). The centrifuge (Multifuge 1S-R), nanoLC (Ultimate™ 3000 RSLCnano), and mass spectrometer (Orbitrap Fusion) were commercially available from Thermo Fisher Scientific (San Jose, CA, USA).

2.2 Fabrication of phos-trap columns

In a glass tube, 6 μL GLYMO was slowly added to 750 μL potassium silicate solution (40 degrees Baume, 3.3 modulus) with magnetic stirring of 800 rpm. The stirring was continued for 30 min to completely dissolve GLYMO in the solution. Then, 15 mg $ATPNa_2$ dissolved in 150 μL water was slowly added to the mixture. After 30 min of stirring, 60 μL formamide mixed with 50 μL water was added to the solution. A fused silica capillary (150 μm I.D., 360 μm O.D.) of 15 cm length was filled with the above solution and incubated in an oven at 60 °C for 5 h and then 90 °C for 12 h. The resulting phos-trap column was trimmed at both ends to a final length of 10 cm and stored in a cool, dry place. The characterization and testing of enrichment performance of the phos-trap are described in the ESI.†

2.3 Design, optimization, and evaluation of the automated online platform

The automated online analytical platform for phosphoproteomic analysis was designed based on an UltiMate™ 3000 RSLCnano system and a high-resolution tandem mass spectrometer (Orbitrap Fusion) with modified connection and operation, the details of which are shown in Fig. 1. The nanoLC was updated with a 250 μL syringe upgrade kit to give a larger injection volume. The solvent for the loading pump was 2% ACN and 0.1% FA. The binary high-pressure gradient pump (NC pump) solvent A was 2% ACN and 0.1% FA, while solvent B was 80% ACN and 0.1% FA. Sample bottles containing 20 mM $ZrCl_4$ solution, sample buffer (protein digest dissolved in 80% ACN and 3% TFA), washing buffer (80% ACN and 3% TFA), elution buffer (1 M $NH_4H_2PO_4$), and cleaning solution (40% ACN and 5% NH_4OH) were placed in a vial tray of the autosampler. The phos-trap column was installed between the outlet of the autosampler and the 10-port valve. The C18 pre-column and the C18 analytical column were mounted on the 10-port valve. The following five-step sequence was executed *via* a job queue by the Xcalibur software. In steps 1–3, 40 μL 20 mM $ZrCl_4$ solution, 50 μL sample buffer, 125 μL washing buffer (twice) were successively injected by the autosampler and pumped through the phos-trap column using the loading pump at a flow rate of 10 μL min^{-1} (10–20 bar). In step 4, the 10-port valve switching to connect the phos-trap column and C18 pre-column, 125 μL elution buffer was injected and pushed through the phos-trap column for retention on the C18 pre-column, with an extended 10 min flush with loading solvent (2% ACN, 0.1% FA) to remove residual salts on the C18 pre-column. In Step 5, the 10-port valve switching back and a mobile-phase gradient controlled by the binary NC pump flowed through the tandem of C18 pre-column and C18 analytical column for phosphopeptide separation; the eluent of the analytical column was directed to the nanospray emitter for online MS/MS analysis. In the meantime, 40 μL of cleaning solution was injected into the phos-trap column to thoroughly rinse it in preparation for the next cycle.

Casein and BSA samples were used for method optimization, the details of which are available in the ESI.† Preparation of protein digests including those of HeLa cells and maize seedlings is also detailed in the ESI.†

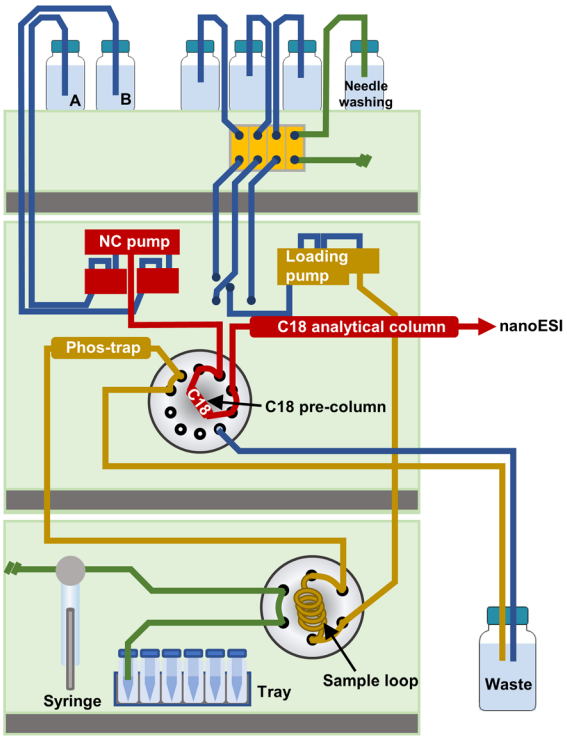

Step	Task	Valve Position
Step 1	Loading Zr^{4+}	1-10
Step 2	Loading peptides	1-10
Step 3	Washing	1-10
Step 4	Elution	1-2
Step 5	Gradient analysis	1-10

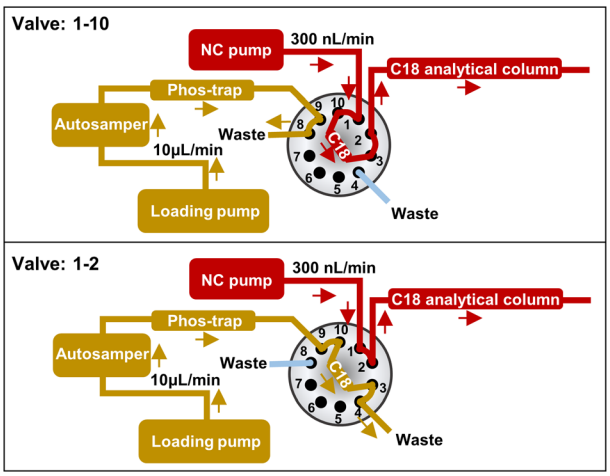

Fig. 1 Design of the automated online platform for phosphoproteomics analysis. The whole analysis process can be divided into two stages: automatic enrichment and gradient analysis. By steps 1–3, the phosphopeptides are enriched by the phos-trap column, while the non-phosphopeptides are excluded during washing. In step 4, the 10-port valve switches to connect the phos-trap column with a C18 pre-column. By a special eluent, the enriched phosphopeptides are eluted from the phos-trap column and reloaded onto the C18 pre-column. The following gradient analysis for phosphopeptides is roughly similar to conventional phosphoproteomic analysis.

2.4 Phosphoproteome of HeLa cells and maize seedling

The analyte (100 μg HeLa cell digest or 200 μg maize digest) was dissolved in 50 μL of loading buffer. As previously described, the enriched phosphopeptides were resolved on a C18 analytical column (75 μm I.D. × 150 mm, 3 μm, 164568, Thermo Fisher Scientific, USA) using a 90 min ACN gradient (6%–25% ACN, 0–85th min; 25%–40% ACN, 85th–90th min) at a flow rate of 300 nL min^{-1}. The mass spectrometer was operated in the data-dependent acquisition (DDA), positive ionization mode. The source voltage was 2.0 kV. The temperature of the ion transfer tube was 320 °C. The MS^1 scans were acquired by the Orbitrap detector (*m*/*z* 300–1400, resolution 120 K, RF lens 60%, AGC target 5.0E5, maximum ion injection time 50 ms). MS^2 scans were acquired by the Ion Trap detector (intensity threshold 5.0E3, include charge state 2–6, exclusion duration 30 s, maximum ion injection time 35 ms, isolation window 2.0 Da, HCD collision energy 32%, scan rate Rapid, AGC target 5.0E3, duty cycle time 3 s). The background ion $(Si(CH_3)_2O)_6H^+$ of *m*/*z* = 445.1200 was used for internal calibration (lock mass).

Peptides in the technical replicates were identified and label-free quantified (LFQ) using Proteome Discoverer™ 2.4, with SEQUEST as the search engine. The raw files of HeLa cells were searched against the FASTA file of *Homo sapiens* in Swiss-Prot (UP000005640). The raw files of maize samples were searched successively against the FASTA files of Zea mays in EPSD[13] (Zea mays) and UniProt (UP000007305). As there are many redundant proteins of Zea mays in the Uniprot database, identification was based primarily on the EPSD search results, with the UniProt search results as supplementary. Trypsin was selected as the enzyme with 2 maximum missed cleavages. Precursor mass tolerance was 10 ppm (Orbitrap). Fragment mass tolerance was 0.2 Da (ion trap). Oxidization (M) and phosphorylation (S, T, Y) were set as variable modifications. Carbamidomethylation (C) was selected as a static modification. The peptide validator calculated false discovery (FDR) rates for peptide groups based on the quality algorithm of the percolator node in the processing workflow. The FDR threshold for high-confidence proteins was 0.01, and for medium-confidence proteins was 0.05. Only phosphorylated peptides were used for calculating protein abundances. Phosphorylation sites were localized and scored by phosphoRS[14] with a default probability cutoff of 0.75.

3. Results and discussion

3.1 Fabrication, characterization, and testing of the phos-trap column

The IMAC materials for phosphopeptide enrichment are typically composed of matrix, chelators and metal ions. There are

also other properties affecting the enrichment performance and efficiency, namely hydrophilicity, surface area, pore size, isoelectric point (IEP), particle size, and magnetic properties. For these reasons, the synthesis of IMAC materials often requires complex procedures, and is accompanied by the use of organic solvents.[15,16] On the other hand, although IMAC materials are currently available in different forms such as microspheres, magnetic beads, or micro-extraction columns, which provide some convenience, they are generally disposable and used offline, producing a certain amount of organic solvents, consumables, or other wastes. Considering such problems, a goal of this work was to develop an affinity column with simple preparation, good reusability and low solvent consumption for online enrichment of phosphopeptides.

As nano-LC-MS/MS is the core instrumentation for proteomics, we envisioned that a most-valued automated technology will need to be based on a widely available version of such a system that incorporates a suitable affinity column for phosphopeptides. Nano-LC requires capillary affinity columns (75–150 μm I.D.). However, most of the existing affinity materials are not amenable to capillary LC work due to poor stability resulting in high backpressure. Therefore, we fabricated a functionalized monolithic column (named as phos-trap column) *via* a "one-pot" process. Key details of the fabrication process and enrichment mechanism of the phos-trap column are illustrated in Fig. S1.† Specifically, the "one-pot" process can be divided into two stages. In the first 5 h, a temperature of 60 °C favored the linking of GLYMO and ATP through an amino-epoxy reaction to form the derivation agent GLYMO–ATP. During the subsequent 12 h of incubation at 90 °C, mesoporous silica was formed *in situ* by hydrolysis and polycondensation of potassium silicate, and was simultaneously functionalized by the derivatization reagent GLYMO–ATP. The triphosphate groups of ATP were employed as highly efficient chelating ligands to immobilize Zr^{4+} ions for enriching phosphorylated peptides from cell/tissue digests.[15] It is worth emphasizing that fabricating the phos-trap columns consumed no organic solvent and little feedstock, and had a low cost and no waste.

The porous structure of the phos-trap column was characterized by scanning electron microscopy (SEM). SEM images revealed that the monolithic bed was well-formed having large through-pores and bonding to the inner wall of the capillary (Fig. S2A and S2B†). The porosity of this monolithic column was also demonstrated by the low backpressure (<30 bar) at a solvent flow rate of 10 μL min^{-1}, thereby making it feasible for the loading pump to push the eluent through the phos-trap column and C18 pre-column (Fig. S2C†). The elemental composition of the monolith was measured by energy dispersive X-ray spectroscopy (EDX). As shown in Fig. S2D,† the monolith was composed of C, N, O, Si, P, and Zr. The existence of N, P and Zr demonstrated successful modification of ATP and Zr^{4+} on the monolith surface.

Fourier-transform infrared spectroscopy (FTIR) was further employed for qualitative characterization as shown in Fig. S3.† The strong and wide characteristic absorption peak at 1077 cm^{-1} was attributed to the asymmetric stretching vibration of Si–O–Si; the peak at 791 cm^{-1} was assigned to Si–O symmetrical stretching vibration; the peak at 469 cm^{-1} was ascribed to Si–O bending vibration; the O–H stretching peak of the surface hydroxyl groups was also observed at 3424 cm^{-1}. After modification with GLYMO–ATP, the 1637 and 1598 cm^{-1} bands from the vibrations of C–N and C–C bonds in the imidazole ring of ATP were evident. The peaks located at 2925 cm^{-1} and 2850 cm^{-1} were ascribed to the stretching vibration of C–H in the alkyl group. After the chelation of Zr^{4+}, a new adsorption peak appeared at 560 cm^{-1} as a result of Zr–O–Zr stretching.[17] It should be pointed out that the characteristic peaks of P–O overlapped with the strong Si–O–Si adsorption peak near 1077 cm^{-1}.

In addition, zeta potential analysis was performed in an acidic solution (pH = 3.0) to monitor changes in the surface potential induced by different degrees of functionalization. As shown in Fig. S4,† H_3O^+, as the predominate ion, would be adsorbed on the surface of silica gel, causing a zeta potential of 24.1 mV. The functionalization of GLYMO-ATP on the surface slightly raised the zeta potential to 27.0 mV. Despite being negatively charged, the triphosphate groups help to adsorb more hydronium ions in the slipping plane, thereby increasing the zeta potential. When high-valent Zr^{4+} ions were immobilized by ATP, the total positive charge density of the slipping plane was further increased, resulting in a significant increase in the zeta potential to 33.2 mV. Taken together, the above chemical characterizations demonstrated that we successfully synthesized the functionalized monolithic column as described in Fig. S1.†

To further investigate the selective enrichment capability of the phos-trap column for phosphopeptides, we employed an elementary setup in which the phos-trap column was used to enrich phosphopeptides from peptide mixture flowing through (Experimental section of ESI†). After washing to remove non-specific non-phosphopeptides, the enriched phosphopeptides were eluted by a solution of 5% NH_4OH and detected with nanoESI-MS. An α-casein digest – comprised of a mixture of non-, mono- and multi-phosphorylated peptides – was used as the analyte for characterization. In the MS spectrum of the α-casein digest without enrichment, abundant non-phosphopeptides dominated the spectrum and only two relatively weak phosphopeptides (*m*/*z* 830.90 and 976.48) were observed, which was a result of signal suppression by non-phosphorylated peptides (Fig. 2A). In contrast, with enrichment of phosphopeptides isolated by the phos-trap column, they dominated the mass spectrum, and virtually all of the non-phosphopeptides disappeared (Fig. 2B); this demonstrates the specificity of the phos-trap column for phosphopeptides. Moreover, an ideal IMAC material also needs to possess high load capacity in order to reduce target loss. Therefore, we next investigated the loading capacity of the phos-trap column. A total of 50 μg α-casein digest, far exceeding the amounts of phosphoproteins (~1 μg) in a typical analysis, was loaded onto the phos-trap column. The entire process of peptide loading, washing, and elution was continuously monitored by MS. The

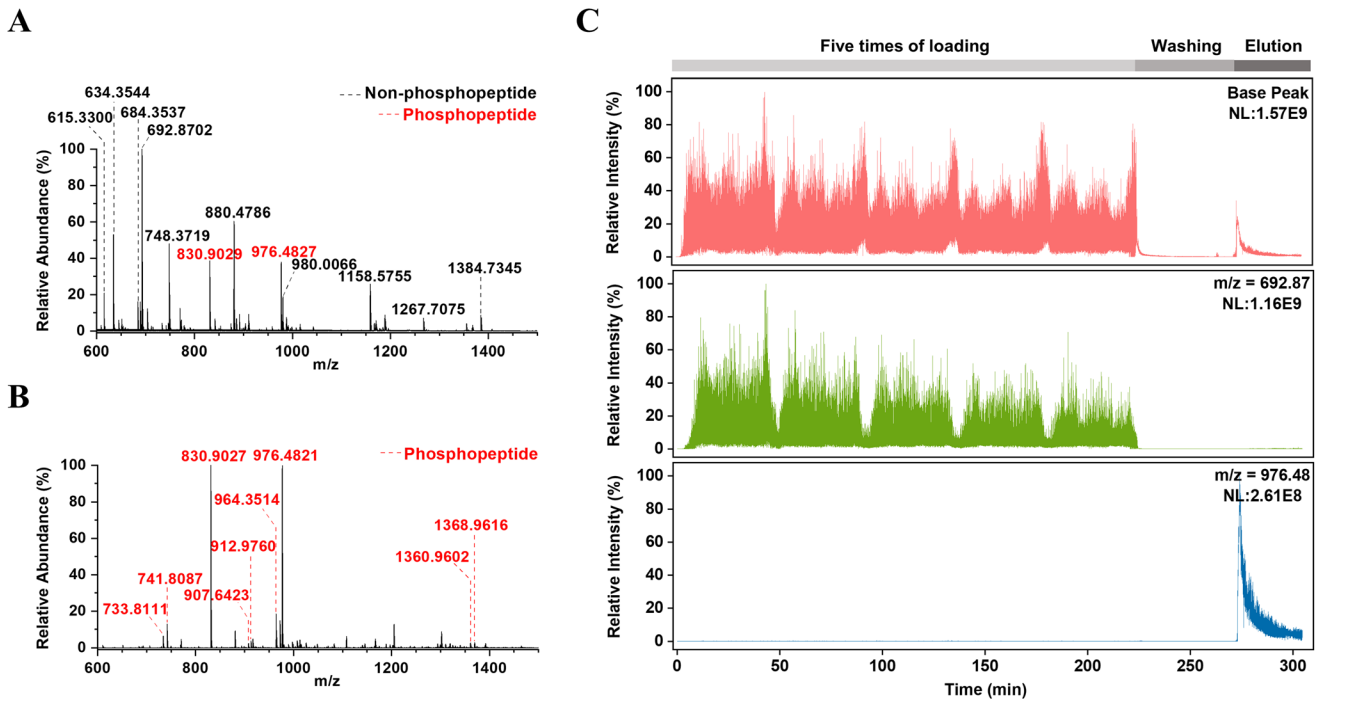

Fig. 2 The enrichment capacity of phos-trap column for phosphopeptides using standard α-casein. (A) Mass spectrum of the α-casein digest without enrichment. (B) Mass spectrum of the α-casein digest after enrichment. (C) Ion chromatograms of the base peak, a typical non-phosphopeptide (*m*/*z* 692.87) and a phosphopeptide (*m*/*z* 976.48) covering peptides loading, washing, and elution during an enrichment process. Note that phosphopeptides are marked with red color in panels A and B.

ion chromatograms of the base peak (the most intense peak in each scan), a representative non-phosphopeptide (*m*/*z* 692.87) and a representative phosphopeptide (*m*/*z* 976.48) are shown in Fig. 2C as an illustration of the efficiency of the enrichment process. During the injection and washing stages, the phosphopeptide (*m*/*z* 976.48), which can be directly detected from the α-casein digest (Fig. 2A), was absent in the eluent (middle panel of Fig. 2C); only non-phosphopeptides were found in the effluent. Phosphopeptides were not eluted until a solution of 5% NH_4OH passed through the phos-trap column (see the bottom panel of Fig. 2C). Taken together, it is evident that the phos-trap column possesses high loading and strong binding capacity for phosphopeptides due to the use of a strong chelating agent (ATP) and high-valence metal ions (Zr^{4+}),[15] as well as a more efficient "one-pot" fabrication process.

In terms of environmental protection, reusable affinity columns significantly reduce costs and environmental pollution compared to disposable columns. Considering the environmental impact of disposable columns and the potential for column regeneration, the recyclability and service life of the phos-trap were investigated. A phos-trap column was used for 50 consecutive cycles of phosphopeptide enrichment from an α-casein digest, followed by a two-month application using different complex biological samples. In the latter stage, we also used an α-casein digest to test the performance of the phos-trap column. The four mass spectra obtained at different time points (the 1st and 50th cycles, one month and two months after being applied to biological samples, respectively) were compared. As shown in Fig. S5,† there was no significant difference in the identities and intensities of enriched phosphopeptides ions. In addition, we also tested the shelf life using the same batch of phos-trap columns. A single phos-trap column stored under cool, dry conditions showed consistent performance compared to columns produced in the same batch over a nine-month interval (Fig. S6†). These data demonstrate the robust reusability and high fidelity of the phos-trap for phosphopeptide enrichment.

3.2 Design and optimization of the online platform

With the development of proteomics aimed at large-scale tasks and continuous increases in labor and material costs, automation is a major trend in technology development. At the same time, a low-carbon economy urges us to minimize waste production during the analysis process. In the field of phosphoproteomics, automated, online, and eco-friendly analysis technology is expected to have broad appeal. Although ours is not the first investigation attempting online phosphoproteomic analysis, previous trials have not attained superior performance: some only implemented semi-automatic online analysis,[18,19] while others identified only a limited number of phosphorylation sites even with prior sample fractionation.[20,21] To our knowledge, there is no published report of automated online technology that can characterize thousands of phosphopeptides in a "single-shot" analysis.

Considering the current shortcomings of online phosphoproteomics, we developed an automated online platform for

phosphoproteomic profiling. The ability to incorporate and integrate the phosphopeptide enrichment directly into a commercially available and widely used analytical platform makes this enrichment methodology valuable to the proteomic community. To this end, we designed an automated online platform based on an UltiMate™ 3000 RSLCnano System and a high-resolution mass spectrometer (Orbitrap Fusion) with modified connections and operations (Fig. 1). Under the precise control of autosampler and 10-port valve, the sample loading, washing, elution, and desalting necessary in enrichment can be automatically implemented. The phosphopeptides enriched by the phos-trap column were eluted onto the C18 pre-column by a special eluent. The following gradient analysis for phosphopeptides is roughly similar to a conventional phosphoproteomic analysis.

A key to realizing a genuine online analytical platform lies in the efficiency of the eluent in eluting enriched phosphopeptides from the phos-trap column to a downstream C18 pre-column for subsequent LC-MS/MS analysis. On account of the viable pH range of C18, eluents containing NH_4OH or $(NH_4)_3PO_4$ were not amenable to the online technology developed. In the present study, three possible eluents for the phos-trap (125 μL each of 1 M $NH_4H_2PO_4$, 50 mM NH_4HCO_3, and 100 mM $ATPNa_2$) were tested for the following reasons. The weakly alkaline 50 mM NH_4HCO_3 may suppress binding between the immobilized Zr^{4+} ions and phosphorylated groups. The $NH_4H_2PO_4$ (pH ~4.0) and $ATPNa_2$ (pH ~3.5) eluents may compete with phosphopeptides for binding with Zr^{4+}. The α-casein digest was used as the analyte, and the phosphopeptides loaded onto the C18 pre-column were eluted with 50% ACN and 0.1% FA for MS detection. The results showed that all three kinds of eluents successfully eluted many mono- and multi-phosphorylated peptides from the phos-trap column but with differences in signal intensity. The highest signals for multi-phosphorylated peptides were obtained with 1 M $NH_4H_2PO_4$ as the eluent (Fig. S7†). It is important because multi-phosphorylated peptides are generally considered more difficult to elute due to high binding affinities, thereby leading to limited coverage of the phosphoproteome.[22] To date, only a few studies have successfully extended coverage of multi-phosphorylated peptides.[23–25] In this work, this property is mainly attributed to three factors. The hydrophilicity of the ATP-modified surface[26] and preference of Zr^{4+} ions[27] facilitated the enrichment of multi-phosphorylated peptides on the phos-trap column. The phosphate in the eluent may also lessen mutual repulsion effects, thereby improving the retention of hydrophilic peptides on the C18 pre-column. Based on our results, 1 M $NH_4H_2PO_4$ was eventually chosen as the best eluent for this work. In addition, other evaluations of this eluent were also implemented. The phosphorylated peptides enriched on the phos-trap column underwent two consecutive elutions and detections, resulting in signal intensities that differed by approximately 10-fold (Fig. S8†), revealing an elution efficiency of about 90% when using 1 M $NH_4H_2PO_4$. To assess whether 1 M $NH_4H_2PO_4$ affects peptide loading on the C18 column, the α-casein digest was separately dissolved in 0.1% FA and 1 M $NH_4H_2PO_4$ and loaded on the C18 pre-column, followed by elution and mass spectrometry detection. There was no apparent difference in the intensity of peptides, especially, phosphopeptides (Fig. S9†), indicating that 1 M $NH_4H_2PO_4$ did not interfere with peptide loading on the C18 pre-column.

As loading and washing conditions often impact the affinity and selectivity of IMAC resins for phosphopeptides,[28] a mixture of digested α-casein and BSA with a mass ratio of 1 : 100 was used as the sample to optimize the phos-trap column for enrichment efficiency, selectivity, and phosphosite coverage. Several parameters that have previously been shown to affect the retention behavior of phosphopeptides and inhibit the binding of carboxyl residues,[28] including the concentrations of ACN and TFA, and the inclusion of 2,5-dihydroxybenzoic acid (DHB) or lactic acid (LA), were investigated. The results are shown in Fig. S10.† Among these, the two eluents containing 1% TFA as loading and washing conditions resulted in the fewest phosphopeptides and were accompanied by the interference of high-intensity non-phosphorylated peptides (m/z 820.07 and 1229.60, corresponding to a non-phosphopeptide with six acidic residues). This was improved when the TFA was raised to 3%. In addition, increasing the ACN concentration from 50% to 80% favored higher phosphopeptide signals. Increasing TFA from 3% to 5% or adding DHB or LA in the loading and washing buffer resulted in insignificant changes. To avoid potential corrosion or blockage of components in the nano-LC caused by high concentrations of acids or salts, we chose to employ the milder buffer containing 80% ACN with 3% TFA as optimal for loading and washing in the following study.

3.3 Performance evaluation of the online platform

We previously demonstrated the high affinity and loading capacity of phos-trap column for phosphopeptides by an elementary setup. However, this setup was not sufficient to prove the capability of this online platform for phosphoproteomic research. Due to the low abundance and low ionization efficiency of phosphopeptides and signal suppression by non-phosphopeptides, the phosphosite coverage, detection limit, and selectivity are key parameters for evaluating the IMAC materials.[9] Moreover, a wide linear range that spans the range of analyte concentrations is also important for quantification. Therefore, standard α-casein and BSA were used as phosphoprotein and non-phosphoprotein respectively, to investigate the above performance parameters of the established platform.

A 1 pmol α-casein digest was used as the sample to assess the phosphosite coverage of this platform. Many mono- and multi-phosphorylated peptides of α-casein were detected with high relative abundance under optimized conditions. A total of 18 out of 19 known sites (95%) of phosphorylation were observed (Fig. 3A and Table 1). This observed property of high site coverage can facilitate the discovery of more phosphorylation events in real samples.

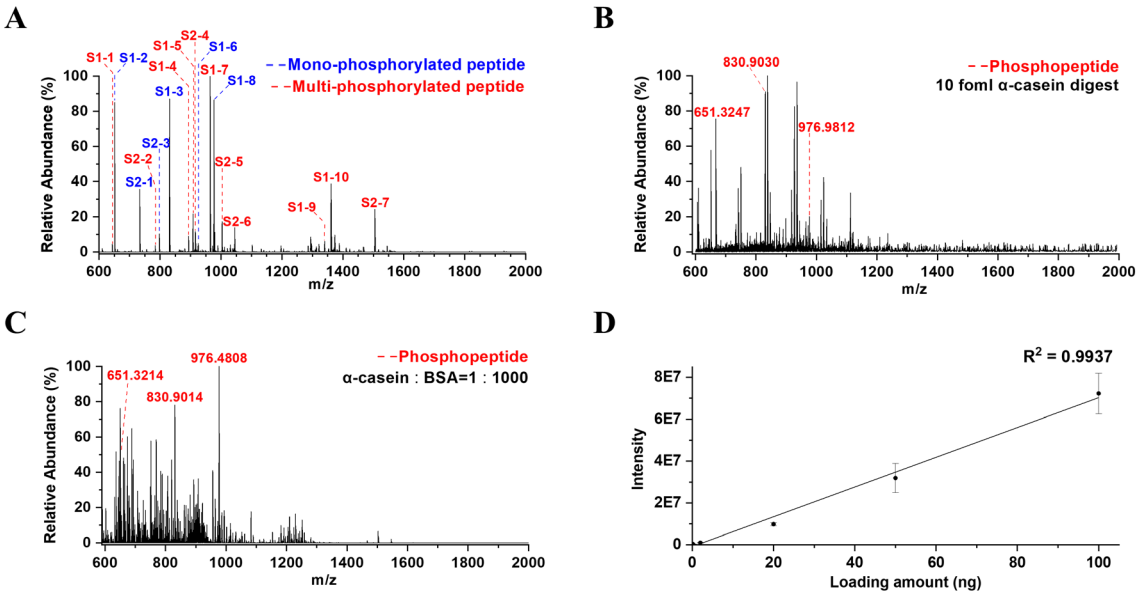

Fig. 3 Performance evaluation of the platform by standard proteins. (A) Mass spectrum of 1 pmol α-casein digest as an analyte. (B) Mass spectrum of 10 fmol α-casein digest as an analyte. (C) Mass spectrum of a mixture of α-casein and BSA digests at a weight ratio of 1 : 1000 as the analyte. (D) Linear range of the platform for quantification, with intensities of a typical phosphopeptide (*m*/*z* 830.90) as the *Y*-axis.

Table 1 The matching results of phosphopeptides enriched by phos-trap column

Protein	No.	Charge	*m*/*z* (obs.)	*m*/*z* (theo.)	Δ*m*/*z* (ppm)	Position	Phosphorylation sites	Peptide sequence
α-casein-S1	S1-1	3	643.2386	643.2354	5.0	58–73	61, 63	DIGSESTEDQAMEDIK
	S1-2	3	651.3258	651.3223	5.4	119–134	130	YKVPQLEIVPNSAEER
	S1-3	2	830.9047	830.9007	4.8	121–134	130	VPQLEIVPNSAEER
	S1-4	3	893.3505	893.3458	5.3	52–73	56, 61, 63	VNELSKDIGSESTEDQAMEDIK
	S1-5	3	907.6469	907.6425	4.8	74–94	79, 81, 82, 83, 90	QMEAESISSSEEIVPNSVEQK
	S1-6	2	924.3703	924.3663	4.3	58–73	61 or 63	DIGSESTEDQAMEDIK
	S1-7	2	964.3536	964.3494	4.4	58–73	61, 63	DIGSESTEDQAMEDIK
	S1-8	2	976.4845	976.4799	4.7	119–134	130	YKVPQLEIVPNSAEER
	S1-9	2	1339.5196	1339.5151	3.4	52–73	56, 61, 63	VNELSKDIGSESTEDQAMEDIK
	S1-10	2	1360.9668	1360.9601	4.9	74–94	79, 81, 82, 83, 90	QMEAESISSSEEIVPNSVEQK
α-casein-S2	S2-1	2	733.8133	733.8096	5.0	153–164	158	TVDMESTEVFTK
	S2-2	4	783.8086	783.8044	5.4	16–39	23, 24, 25, 28	KNTMEHVSSSEESIISQETYKQEK
	S2-3	2	797.8609	797.8571	4.8	152–164 or 153–165	158	KTVDMESTEVFTK or TVDMESTEVFTKK
	S2-4	3	916.3377	916.3381	0.4	16–36	23, 24, 25, 28	KNTMEHVSSSEESIISQETYK
	S2-5	3	1003.3539	1003.3480	5.9	61–85	71, 72, 73, 76	NANEEEYSIGSSSEESAEVATEEVK
	S2-6	3	1044.7422	1044.7368	5.2	16–39	23, 24, 25, 28	KNTMEHVSSSEESIISQETYKQEK
	S2-7	2	1504.5288	1504.5184	6.9	61–85	71, 72, 73, 76	NANEEEYSIGSSSEESAEVATEEVK

To determine the detection limit of this online platform, the digest of trace amounts of α-casein (10 fmol and 100 fmol) was utilized. As shown in Fig. 3B and Fig. S11B,† five phosphopeptides were detected in the 100 fmol α-casein digest sample, and three of these were still observed in 10 fmol of the digest. The detection limit of this platform is superior to those reported in offline enrichment methods (Table S1†).

The mixtures of α-casein and BSA digests in molar ratios of 1 : 500 and 1 : 1000 were used to assess selectivity; the low proportion of the α-casein *versus* BSA was used to simulate the low-abundance phosphopeptides in biological samples. Phosphopeptides dominated the spectrum when the molar ratio was 1 : 500 (Fig. S11C†), but three phosphopeptides could still be detected when the BSA molar ratio was doubled to 1 : 1000 (Fig. 3C). Although limited by the volume of washing solution, the selectivity of the platform toward phosphopeptides was able to compete with advanced offline enrichment methods.[9,10]

Many quantitation studies focus on sensitivity and selectivity while ignoring the linear range in assessing enrichment methods in phosphoproteomics. Therefore, we also evaluated the linear range of this platform employing a series of injections of 0 ng, 0.2 ng, 2 ng, 20 ng, 50 ng, 100 ng, 150 ng, and 200 ng of α-casein digest. Plotting the intensity of a typical phospho-

peptide (m/z = 830.90) against the amount injected, the regression and linearity were acceptable (R^2 = 0.994) within the quantity range of 0 ng to 100 ng (Fig. 3D), which should encompass most detectable phosphoproteins in biological samples.

3.4 The applications of the online platform to biological samples

Encouraged by the remarkable performance of the phos-trap column with standard proteins, we further applied this platform to the analysis of two biological samples, namely HeLa cells and maize seedlings (representing phosphopeptides from animal sources and plant sources, respectively). Three replicate analyses were performed on the same sample under the same operating conditions and acquisition parameters.

A total of 6575 phosphorylation sites in 5229 phosphopeptides, belonging to 1695 phosphoproteins, were identified in HeLa cell digests based on LFQ (Fig. 4A–C, Supplementary Data 1–3†). Similarly, 3741 phosphorylation sites in 3123 phosphopeptides from 1579 phosphoproteins were characterized from maize seedling digests (Supplementary Data 6–8†). A summary of the identification results through different methods is listed in Table S2.† Remarkably, many multi-phosphorylated peptides were observed, with about 64% of the total phosphopeptides in HeLa cells and 51% in maize seedlings possessing more than a single phosphosite. We also found that a significant number of the phosphopeptides were observed in different phosphorylation states (on different residues or having different numbers of phosphorylation), which accounts for 20% in HeLa cells and 14% in maize sequences (Fig. 4D and Supplementary Data 4, 9†).

Phosphorylation sites were localized and scored by phosphoRS[14] with a default probability cutoff of 0.75. Even when we applied a stricter probability cutoff of 0.95, we still observed 5311 (as opposed to 6575) highly confident phosphorylation sites in HeLa cells. Comparing the phosphosites identified herein with the 342 555 known human phosphorylation sites integrated from three databases (PhosphoSitePlus,[29] qPhos,[30] and a newly published work[31]), we conclude that 120 phosphorylation sites discovered in our work are new and have never been reported (Fig. 4E and Supplementary Data 5†). In addition, we discovered 588 novel phosphorylation sites in maize by comparing our data with the known 43 969 phosphosites compiled in EPSD[13] (the Eukaryotic Phosphorylation Site Database, a comprehensive data resource of experimentally identified phosphorylated sites from 68 eukaryotes) (Fig. 4F and Supplementary Data 10†).

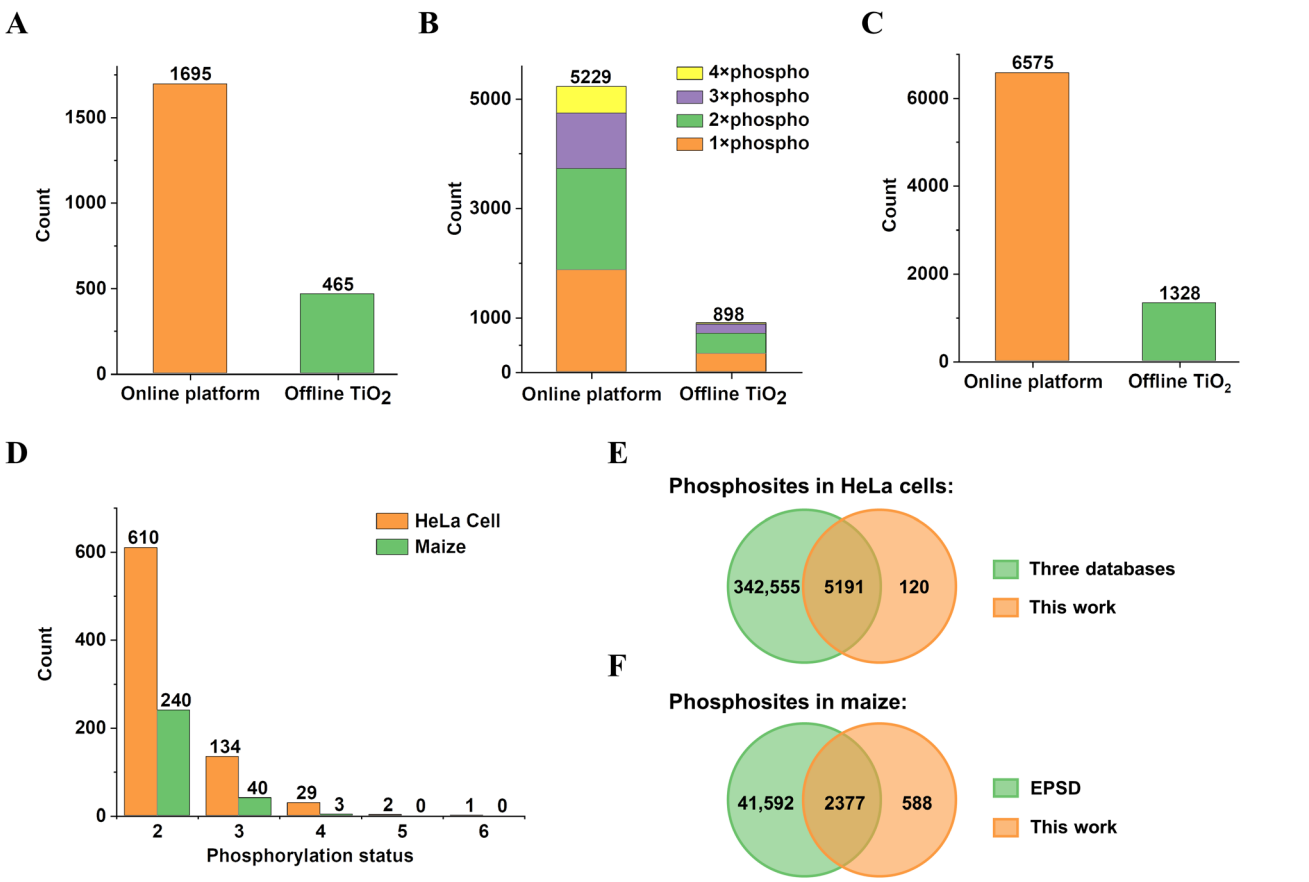

Fig. 4 Phosphoproteomics profiling of HeLa cells by the online platform and offline TiO_2 enrichment based on label-free quantitation (LFQ). (A) Identified and quantified phosphoproteins; (B) identified and quantified phosphopeptides; (C) identified phosphorylation sites. (D) Peptides in different phosphorylation states identified by the online platform. Newly discovered phosphorylation sites in HeLa cells (E) and maize seedling (F) in this work.

For a technical comparison, commercial TiO_2 was used to enrich phosphopeptides offline. The phosphopeptides eluted from TiO_2 using 40%ACN with 5%NH_4OH were analyzed with the same optimal LC gradient and acquisition parameters after acidification, volatilization, and desalting steps as described before. In general, there were 3 to 5 times more phosphopeptides and phosphoproteins identified using the online analytical platform technology developed herein than the offline TiO_2 enrichment (Fig. 4A–C and Supplementary Data 11†). Additionally, the current online analytical platform technology performed better in the identification of multi-phosphorylated peptides, leading to the observation of significantly more phosphopeptides.

The reproducibility of this online analytical platform technology is excellent and apparent in the following observations: (1) very similar base peak chromatograms (Fig. 5A and Fig. S12A†) were observed for each set of three identical runs; (2) over 94% of the phosphopeptides and 96% of the phosphoproteins were detected and quantified in all triplicates (Fig. 5B and Fig. S12B†); and (3) low variation in quantification between each replicate was reflected by the high Pearson correlation values of 0.95–0.98 for phosphopeptides and 0.97–0.98 for phosphoproteins (Fig. 5C and Fig. S12C†). Taken together, the consistent qualitative and quantitative results are reflective of the high reproducibility of our online analytical platform technology.

Compared with recent reports of offline enrichment,[16,25,32–37] the performance of our online analytical platform technology was competitive in different aspects (Table S1†). In addition, the quantitative reproducibility of this method was better with a correlation coefficient R^2 of 0.95 compared to the R^2 of 0.89 obtained for offline enrichment in a recent work,[38] and was even comparable to its offline data-independent acquisition (DIA) method (R^2 = 0.93). Use of the above comparison should be exercised with caution as it cuts across different studies and laboratories. However, the better performance observed herein with the online analytical system is in keeping with its more precise control of experimental parameters, including injection volume and flow rate, thereby reducing the variability in enrichment and resulting in more reproducible results.

We put forward a feasible strategy to increase the throughput by achieving simultaneous enrichment and gradient LC-MS analysis (Fig. S13†). In this way, the cycle time of this online platform can be only 5 min longer than that of a general proteomic analysis, which is less than 5% of the total time.

3.5 Ability to characterize peptides in different phosphorylation states in biological samples

Due to their low abundances, multi-phosphorylated peptides are challenging for phosphoproteomics.[23–25] The online analytical platform technology that we have developed displays efficient enrichment for both mono- and multi-phosphorylated peptides, the latter of which was evident by their relative abun-

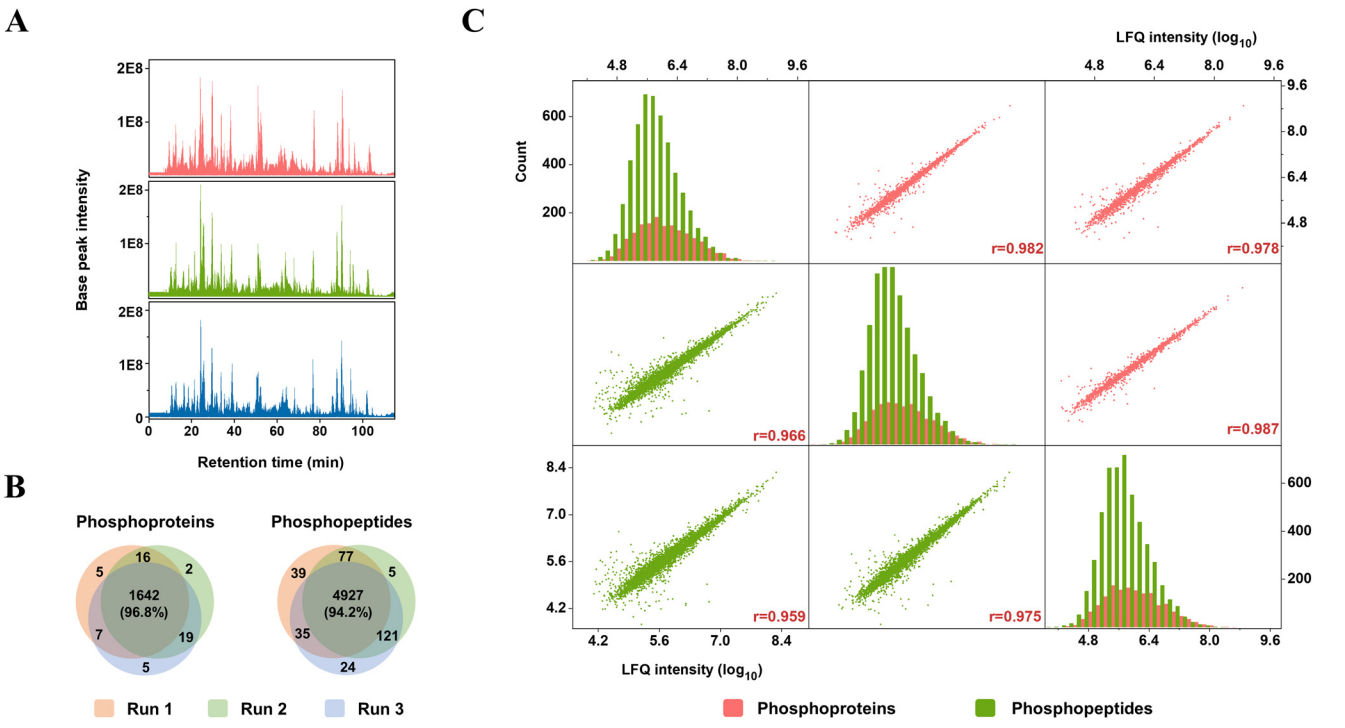

Fig. 5 The reproducibility evaluation of the online platform. (A) Base peak comparison of the three parallel runs. (B) Two Venn diagrams of identified phosphoproteins and phosphopeptides in HeLa cells by three parallel runs, respectively. (C) Scatter plots of abundances of the phosphoproteins (upper-right) and phosphopeptides (lower-left) in log_{10} scale between replicates, and histograms of the abundances in log_{10} scale of each replicate (middle line).

dance and diversity. Many peptides in different phosphorylation states have been identified (Supplementary Data 4†), which may help elucidate the protein chemistry and phosphorylation/dephosphorylation mechanisms at play. For instance, the cyclic AMP-dependent transcription factor ATF2 can be phosphorylated by five kinases.[39] This work strongly suggests that JNK/P38 and PKA are involved in the phosphorylation of ATF2 in HeLa cells by virtue of the observation of phosphorylation on S62, T69, and T71 (Supplementary Data 4, No. 248 and the visual description in Fig. S14†).

Similarly, the involvement of specific phosphatases can also be inferred from site-specific phosphorylation. For human CARHSP1, observation of phosphopeptides that contain phosphorylation on S30 and S32, as well as on S30, S32 and S41 (Supplementary Data 4, No. 755†), is in accordance with the interpretation that S41 is independently dephosphorylated by an ionomycin-mediated calcium flux.[40] In addition, we found another phosphorylation site on T45 (Supplementary Data 4, No. 754†), which might be independently dephosphorylated by another phosphatase. Phosphorylation status can also distinguish the dual roles of STAT3 as a transcriptional regulator and a modulator of oxidative respiration by the di-phosphorylated (T714 and S727) and mono-phosphorylated (S727) peptides (Supplementary Data 4, No. 294†).[41] The sequential phosphorylation of some proteins, including stathmin[42] and Cep55[43] (Supplementary Data 4, No. 255 and 445†) can similarly be monitored and permits the detection of the inactive, preparatory, and active states of such proteins.

3.6 Ability to discover new phosphorylation sites in biological samples

Benefiting from the high affinity of our platform technology for multi-phosphorylated peptides, 85% of the new phosphorylation sites were discovered in multi-phosphorylated peptides. The 120 new phosphorylation sites from HeLa cells are located in 77 phosphoproteins (Supplementary Data 5†), most of which have been reported to be associated with diseases and key cellular processes. We observed for the first time phosphorylation on ZC3H11B, an eye disease-associated protein.[44]

Many of these proteins have been proven to function through reversible phosphorylation. For instance, the reversible phosphorylation of DBS, RIN1 and APC was related to tumor suppression.[45–48] Phosphorylated XRCC4 and CHD4 are required for the repair of DNA double-strand breaks.[49,50] Reversible phosphorylation of URI triggers adaptive responses of cancer cells under glucose deficiency,[51] while that of PDE3A in human platelets modulates intracellular cAMP levels.[52] Abnormal phosphorylation of FBXW2 promotes tumor formation[53] whereas phosphorylation of RUBCNL controls the maturation of autophagosomes under different nutritional conditions.[54] Reversible phosphorylation of titin modulates the contractile performance of the heart;[55] phosphorylated CENPT and MCRS1 promote the assembly of kinetochores and chromosome segregation during mitosis.[56,57] Ubiquitination-associated enzymes MYCBP2 and UBE2O have been predicted to be regulated by phosphorylation.[58,59] Nevertheless, most of these studies claimed limited understanding of the phosphorylation and regulatory mechanisms. Thus, the use of more powerful tools for the examination of phosphorylation, such as the technology reported herein, will be of great value to better understand phosphorylation and its role in protein activation and function.

4. Conclusions

In this study, we developed an eco-friendly, cost-affordable, and automated online platform for phosphoproteome profiling and characterization. First, a novel and reusable phos-trap column with excellent performance in phosphopeptide enrichment was synthesized by an easy, zero-emission, and "one-pot" process. Next, an automated online analytical platform integrating enrichment, washing, elution, and gradient analysis was established and implemented for the first time, which can significantly minimize the use of chemical reagents, organic solvents, and consumables. Under software control, it can automatically and continuously enrich and analyze phosphopeptides from a batch of biological samples without operator intervention. It achieves results with high reproducibility and deep coverage, thereby facilitating the characterization of peptides with different phosphorylation states and the discovery of novel phosphosites. With the development of phosphoproteomics towards large-scale studies and the advent of a low-carbon economy, this automated online platform for phosphoproteome profiling is expected to advance the research of protein phosphorylation in the future.

Data availability

The raw files and search results are publicly available in iProX (**https://www.iprox.cn/**) with project No. of IPX0003628000.

Author contributions

W. Z. and C. L. conceptualization, investigation and data curation; W. L. resources; W. H. and Q. K. methodology; S. W. software; S. Y. and K. W. M. supervision; W. Z. and S. Y. writing–original draft; K. W. M., A. R. F., and A. C. H. writing–review and editing.

Conflicts of interest

The authors declare no competing interests.

Acknowledgements

This work was jointly supported by grants from the Key Realm R&D Program of Guangdong Province (No. 2020B0202090005 and 2021TQ06N115), the Science and Technology Program of

Guangdong Province (No. 2021A0505030050), the Science and Technology Program of Guangzhou City (No. 202201010564), the Project of Collaborative Innovation Center of GDAAS (XTXM202203), and the Special Fund for Scientific Innovation Strategy-construction of High Level Academy of Agriculture Science (R2021YJ-YB3010; R2020PY-JX019; R2021YJ-YB1004); K. W. M. S. acknowledges funding from the Natural Sciences and Engineering Research Council of Canada for work on developing the enrichment chemistry and materials; Financial support from the program of China Scholarship Council (CSC) (No. 201706770041).

References

1 Y. L. Deribe, T. Pawson and I. Dikic, *Nat. Struct. Mol. Biol.*, 2010, **17**, 666–672.
2 T. E. Thingholm, O. N. Jensen and M. R. Larsen, *Proteomics*, 2009, **9**, 1451–1468.
3 K. Engholm-Keller and M. R. Larsen, *Proteomics*, 2013, **13**, 910–931.
4 S. Liu, H. Chen, X. Lu, C. Deng, X. Zhang and P. Yang, *Angew. Chem., Int. Ed.*, 2010, **49**, 7557–7561.
5 H. Zhou, M. Ye, J. Dong, G. Han, X. Jiang, R. Wu and H. Zou, *J. Proteome Res.*, 2008, **7**, 3957–3967.
6 W. Y. Chen and Y. C. Chen, *Anal. Bioanal. Chem.*, 2010, **398**, 2049–2057.
7 C. T. Chen and Y. C. Chen, *Anal. Chem.*, 2005, **77**, 5912–5919.
8 L. Zhang, Y. Wang, L. Pan, R. Tang, T. Asoh, J. Ou and H. Uyama, *Green Chem.*, 2021, **23**, 7674–7684.
9 H. Zhang, X. Li, S. Ma, J. Ou, Y. Wei and M. Ye, *Green Chem.*, 2019, **21**, 2052–2060.
10 L. Pan, S. Ma, R. Tang, W. Wu, J. Ou, C. Li and Y. Shen, *Green Chem.*, 2022, **24**, 238–250.
11 S. J. Humphrey, O. Karayel, D. E. James and M. Mann, *Nat. Protoc.*, 2018, **13**, 1897–1916.
12 J. G. Abelin, J. Patel, X. Lu, C. M. Feeney, L. Fagbami, A. L. Creech, R. Hu, D. Lam, D. Davison and L. Pino, *Mol. Cell. Proteomics*, 2016, **15**, 1622–1641.
13 S. Lin, C. Wang, J. Zhou, Y. Shi, C. Ruan, Y. Tu, L. Yao, D. Peng and Y. Xue, *Briefings Bioinf.*, 2021, **22**, 298–307.
14 T. Taus, T. Kocher, P. Pichler, C. Paschke, A. Schmidt, C. Henrich and K. Mechtler, *J. Proteome Res.*, 2011, **10**, 5354–5362.
15 L. Zhang, Q. Zhao, Z. Liang, K. Yang, L. Sun, L. Zhang and Y. Zhang, *Chem. Commun.*, 2012, **48**, 6274–6276.
16 Y. Hong, Y. Yao, H. Zhao, Q. Sheng, M. Ye, C. Yu and M. Lan, *Anal. Chem.*, 2018, **90**, 7617–7625.
17 M. Aghazadeh, A. M. Barmi and M. Hosseinifard, *Mater. Lett.*, 2012, **73**, 28–31.
18 H. Yang, C. Deng and X. Zhang, *Talanta*, 2016, **153**, 285–294.
19 S. B. Ficarro, Y. Zhang, M. J. Carrasco-Alfonso, B. Garg, G. Adelmant, J. T. Webber, C. J. Luckey and J. A. Marto, *Mol. Cell. Proteomics*, 2011, **10**(11), DOI: **10.1074/mcp.O111.011064**.
20 S. Lemeer, M. W. Pinkse, S. Mohammed, B. van Breukelen, J. den Hertog, M. Slijper and A. J. Heck, *J. Proteome Res.*, 2008, **7**, 1555–1564.
21 M. W. Pinkse, S. Mohammed, J. W. Gouw, B. van Breukelen, H. R. Vos and A. J. Heck, *J. Proteome Res.*, 2008, **7**, 687–697.
22 T. E. Thingholm, O. N. Jensen, P. J. Robinson and M. R. Larsen, *Mol. Cell. Proteomics*, 2008, **7**, 661–671.
23 H. Zhong, X. Xiao, S. Zheng, W. Zhang, M. Ding, H. Jiang, L. Huang and J. Kang, *Nat. Commun.*, 2013, **4**, 1656.
24 X. Long, Z. Zhang, J. Li, D. Sheng and H. Lian, *Chem. Commun.*, 2017, **53**, 4620–4623.
25 J. Peng, H. Niu, H. Zhang, Y. Yao, X. Zhao, X. Zhou, L. Wan, X. Kang and R. Wu, *ACS Appl. Mater. Interfaces*, 2018, **10**, 32613–32621.
26 L. Zhang, Z. Liang, L. Zhang, Y. Zhang and S. Shao, *Anal. Chim. Acta*, 2015, **900**, 46–55.
27 J. Jiang, X. Sun, Y. Li, C. Deng and G. Duan, *Talanta*, 2018, **178**, 600–607.
28 W. Qiu, C. A. Evans, A. Landels, T. K. Pham and P. C. Wright, *Anal. Chim. Acta*, 2020, **1129**, 158–180.
29 P. V. Hornbeck, B. Zhang, B. Murray, J. M. Kornhauser, V. Latham and E. Skrzypek, *Nucleic Acids Res.*, 2015, **43**, D512–D520.
30 K. Yu, Q. Zhang, Z. Liu, Q. Zhao, X. Zhang, Y. Wang, Z. Wang, Y. Jin, X. Li and Z. Liu, *Nucleic Acids Res.*, 2019, **47**, D451–D458.
31 D. Ochoa, A. F. Jarnuczak, C. Viéitez, M. Gehre, M. Soucheray, A. Mateus, A. A. Kleefeldt, A. Hill, L. Garcia-Alonso and F. Stein, *Nat. Biotechnol.*, 2020, **38**, 365–373.
32 Y. Hong, C. Pu, H. Zhao, Q. Sheng, Q. Zhan and M. Lan, *Nanoscale*, 2017, **9**, 16764–16772.
33 D. Zhen, C. Gao, B. Zhu, Q. Zhou, C. Li, P. Chen and Q. Cai, *Anal. Chem.*, 2018, **90**, 12414–12421.
34 R. Kupcik, J. M. Macak, H. Rehulkova, H. Sopha, I. Fabrik, V. Anitha, J. Klimentova, P. Murasova, Z. Bilkova and P. Rehulka, *ACS Omega*, 2019, **4**, 12156–12166.
35 H. Zheng, J. Zhang, J. Ma and Q. Jia, *ACS Appl. Mater. Interfaces*, 2020, **12**, 57468–57476.
36 I. A. Diez, I. Govender, P. Naicker, S. Stoychev, J. Jordaan and O. N. Jensen, *J. Proteome Res.*, 2020, **20**, 453–462.
37 H. Chu, H. Zheng, N. Sun and C. Deng, *Anal. Chim. Acta*, 2022, 338693.
38 D. B. Bekker-Jensen, O. M. Bernhardt, A. Hogrebe, A. Martinez-Val, L. Verbeke, T. Gandhi, C. D. Kelstrup, L. Reiter and J. V. Olsen, *Nat. Commun.*, 2020, **11**, 787.
39 A. Sevilla, C. R. Santos, F. M. Vega and P. A. Lazo, *J. Biol. Chem.*, 2004, **279**, 27458–27465.
40 J. R. Pfeiffer, B. L. McAvoy, R. E. Fecteau, K. M. Deleault and S. A. Brooks, *Mol. Cell. Biol.*, 2011, **31**, 277–286.
41 M. S. Waitkus, U. M. Chandrasekharan, B. Willard, T. L. Tee, J. K. Hsieh, C. G. Przybycin, B. I. Rini and P. E. DiCorleto, *Mol. Cell. Biol.*, 2014, **34**, 1800–1811.
42 S. Honnappa, W. Jahnke, J. Seelig and M. O. Steinmetz, *J. Biol. Chem.*, 2006, **281**, 16078–16083.

43 M. Fabbro, B. B. Zhou, M. Takahashi, B. Sarcevic, P. Lal, M. E. Graham, B. G. Gabrielli, P. J. Robinson, E. A. Nigg and Y. Ono, *Dev. Cell*, 2005, **9**, 477–488.
44 C. Y. Cheng, M. Schache, M. K. Ikram, T. L. Young, J. A. Guggenheim, V. Vitart, S. MacGregor, V. J. Verhoeven, V. A. Barathi and J. Liao, *Am. J. Hum. Genet.*, 2013, **93**, 264–277.
45 J. Yamauchi, J. R. Chan, Y. Miyamoto, G. Tsujimoto and E. M. Shooter, *Proc. Natl. Acad. Sci. U. S. A.*, 2005, **102**, 5198–5203.
46 S. Ziegler, T. Eiseler, R. P. Scholz, A. Beck, G. Link and A. Hausser, *Mol. Biol. Cell*, 2011, **22**, 570–580.
47 S. Ikeda, M. Kishida, Y. Matsuura, H. Usui and A. Kikuchi, *Oncogene*, 2000, **19**, 537–545.
48 F. Zhang, R. L. White and K. L. Neufeld, *Mol. Cell. Biol.*, 2001, **21**, 8143–8156.
49 M. Terasawa, A. Shinohara and M. Shinohara, *PLoS Genet.*, 2014, **10**, e1004563.
50 G. Smeenk, W. W. Wiegant, H. Vrolijk, A. P. Solari, A. Pastink and H. van Attikum, *J. Cell Biol.*, 2010, **190**, 741–749.
51 S. Burén, A. L. Gomes, A. Teijeiro, M. A. Fawal, M. Yilmaz, K. S. Tummala, M. Perez, M. Rodriguez-Justo, R. Campos-Olivas and D. Megías, *Cancer Cell*, 2016, **30**, 290–307.
52 R. W. Hunter, C. MacKintosh and I. Hers, *J. Biol. Chem.*, 2009, **284**, 12339–12348.
53 J. Xu, W. Zhou, F. Yang, G. Chen, H. Li, Y. Zhao, P. Liu, H. Li, M. Tan and X. Xiong, *Nat. Commun.*, 2017, **8**, 1–16.
54 X. Cheng and Q. Sun, *Autophagy*, 2019, **15**, 1120–1121.
55 F. Koser, C. Loescher and W. A. Linke, *FEBS J.*, 2019, **286**, 2240–2260.
56 K. E. Gascoigne, K. Takeuchi, A. Suzuki, T. Hori, T. Fukagawa and I. M. Cheeseman, *Cell*, 2011, **145**, 410–422.
57 H. Yang, F. Zhang, C. J. Huang, J. Liao, Y. Han, P. Hao, Y. Chu, X. Lu, W. Li and H. Yu, *Mol. Biol. Cell*, 2019, **30**, 1060–1068.
58 N. Malik, R. S. Nirujogi, J. Peltier, T. Macartney, M. Wightman, A. R. Prescott, R. Gourlay, M. Trost, D. R. Alessi and A. Karapetsas, *Biochem. J.*, 2019, **476**, 3081–3107.
59 K. Liang, A. G. Volk, J. S. Haug, S. A. Marshall, A. R. Woodfin, E. T. Bartom, J. M. Gilmore, L. Florens, M. P. Washburn and K. D. Sullivan, *Cell*, 2017, **168**, 59–72.e13.